Synthesis of 3-hexylthiophene derived semiconductor polymers and composites with nanoparticles

Edgar Vaquera[a], Arturo Caballero[a], Fernanda Retana, Susana López-Cortina[b], y Thelma Serrano[a]*

[a]*Universidad Autónoma de Nuevo León, Facultad de Ciencias Químicas, Laboratorio de Materiales I, Av. Universidad S/N, Cuidad Universitaria, 66455, San Nicolás ed los Garza, Nuevo León, MEXICO.*

[b]*Universidad Autónoma de Nuevo León, Facultad de Ciencias Químicas, Laboratorio de Química Industrial, Av. Universidad S/N, Cuidad Universitaria, 66455, San Nicolás ed los Garza, Nuevo León, MEXICO.*

**tserranoq@uanl.edu.mx.*

Recibido 30 octubre 2022, Aceptado 30 noviembre 2022

Abstract
The monomer 3-hexylthiophen-2,5-dicarboxaldehyde was synthetized from precursor 3-hexylthiophene by Vilsmeier-Haack reaction. Three p-type semiconductor polymers (PHT-P, PHT-B and PHT-H) were synthetized by aldol condensation from this monomer with three different ketones (propanone, butanone and hexanone). Three composites were created by adding PbS/ZnS nanoparticles to these polymers. Light absorption increased to the red from polymers to composites. Electrical conductivity increased from 10^{-6} S/cm in polymers to 10^{1} S/cm in composites.

Key words: *polymer, semiconductor, aldol condensation*.

Introduction

Polymers were used for a long time as insulant materials. However, in the last 30 years, we have synthesized polymers with semiconducting properties that have become of great interest to find out new applications for this materials[1]. To the date, these polymers can be classified into four categories: conjugated conducting polymers, charge transfer polymers, ionically conducting polymers, and conductively filled polymers[2].

The conjugated structure or conjugated segments coupled with atoms providing p-orbitals for a continuous orbital overlap (e.g. N, S) is necessary for polymers to become intrinsically conducting, in such a way that it allows the passage of the charge carriers[3-5].

Owing to the delocalization of electrons in continuously overlapped orbitals along the polymer backbone, certain conjugated polymers exhibit interesting optical, electrical and magnetic properties. In addition, semiconductor polymers are flexible, light-weight, cheap and can be synthesized by solution methods, therefore they can be obtained easily and with high reproducibility[6]. These qualities allow them to be used in many applications, including protecting metals from corrosion[7], artificial actuators[8], sensing devices[9], all-plastic transistors[10], solar cells[11-13] and light-emitting displays[14].

Among conducting polymers, polythiophenes and derivatives have acquired high relevance as p-type materials, for their wide range spectra of absorption, good conductivity, high charge carrier mobility and good chemical stability[6]. Among polythiophenes, one of those who have highlighted is poly(3-hexylthiophene), P3HT, primary for its low band-gap energy (E_g), of about 1.9 eV, and good conductivity, greater than 1 $S \cdot cm^{-1}$,[15].

Efforts to achieve lower E_g in these materials have led researchers to modify the structure of P3HT creating more branched backbones or complex rings as bithiophenes and benzothiophenes[16,17].

There are different synthesis methods to prepare semiconducting polymers, among these we found the via electrochemistry[18], Stille reaction[5] and recently the aldol condensation[19]; the latter has the advantage of soft reaction conditions with short times and moderate temperatures, in comparison to other methods. Aldol condensation produces C=C and C=O double bonds, achieving the necessary conjugation in the polymer chain[20], and it is applicable only in molecules containing carbonyl groups.

It is posed that the aldol condensation can generate a polymer like P3HT but with different structures, with greater separation between heterocycle rings and maintaining high conjugation. For this to be achieved it is necessary that 3-hexylthiophene acquires a pair of carbonyl groups to be susceptible for aldol condensation. Vilsmeier-Haack reaction is contemplated to achieve the addition of carbonyl groups to heterocycle[21]. Figure 1.1 shows two initial Vilsmeier-Haack acylation's before the three options of aldol condensation polymerization depending the ketone used.

Apart of p-type material, in photovoltaic devices it is needed a n-type material too, the one who conducts electrons. For this purpose, many nanoparticles had been synthesized. They have also the capability to harvest light, be processable in solution, be reinforced with a shell, and some of them fit with the E_g of the p-material. To obtain better results in a hybrid system a n-type semiconductor must be coupled with values in the energy levels HOMO and LUMO greater than presented by the p-type semiconductor[24], these values are

determined by electrochemical techniques as carried out in this work.

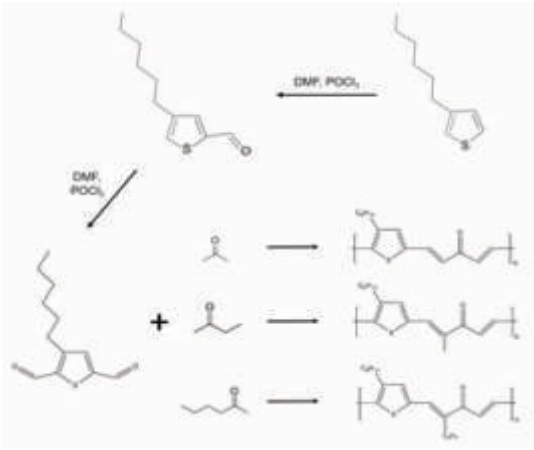

Figure 1. Reactions overview

2. Experiment

2.2 Synthesis of monomer 3-hexylthiophen(2,5-dicarboxaldehyde)

In a two-neck flask closed with rubber septums and nitrogen atmosphere, 3-hexylthiophene and dimethylformamide DMF were added; finally, $POCl_3$ was added dropwise; here, reactants molar relation was 1:1.5:1.5. The system was stirred 1 h at 90 °C. Crude was drawn off with water and neutralized with $NaHCO_3$. A 3-stage extraction was developed with CH_2Cl_2 using 10 mL of it each time. Organic phase was dried in Na_2SO_4 and filtered. This organic blend was labeled as 3HTCHO. This product was carried to a second acylation reaction, increasing equivalents to a 3HTCHO: DMF: $POCl_3$ proportion of 1:4:4. Here, reactants were kept stirred 2 h at 90 °C. After reaction, crude was drawn off, neutralized and dried the same way as in the first acylation. Now, the product was labeled as $3HT(CHO)_2$.

2.3 Synthesis of polymers

2.3.1 poly[2-(1,4-dien-3-one)-4-hexylthiophene] (P3HT-P)

104 mg of monomer $3HT(CHO)_2$ dissolved in tetrahydrofuran/ethanol were heated to 50 °C under reflux. Then 18.5 mg of NaOH dissolved in ethanol were added and finally 26.9 mg of propanone in ethanol dropwise. Molar quantities of $3HT(CHO)_2$-NaOH-propanone were 1:2:1. System were kept 30 min under reflux at 50 °C. Crude were centrifugated to recover the polymer. Supernatant fluid containing a $3HT(CHO)_2$/polymer mixture were separated using CH_2Cl_2 and centrifugation. Polymer was introduced in acid solution and finally washed with water.

2.3.2 poly[2-(2-methyl-1,4-dien-3-one)-4-hexylthiophene] (P3HT-B)

202 mg of monomer $3HT(CHO)_2$ dissolved in tetrahydrofuran/ethanol were heated to 65 °C under reflux. Then 36 mg of NaOH dissolved in ethanol were added and finally 65 mg of butanone in ethanol dropwise. Molar quantities of $3HT(CHO)_2$-NaOH-butanone were 1:2:1. System were kept 45 min under reflux at 65 °C. Crude were centrifugated to recover the polymer. Supernatant fluid containing a $3HT(CHO)_2$/polymer mixture were separated using CH_2Cl_2 and centrifugation. Polymer was introduced in acid solution and finally washed with water.

2.3.3 poly[2-(2-propyl-1,4-dien-3-one)-4-hexylthiophene] (P3HT-H)

1.237 mmol of monomer $3HT(CHO)_2$ dissolved in tetrahydrofuran/ethanol were heated to 65 °C under reflux. Then 2.47 mmol of KOH dissolved in ethanol were added and finally 1.237 mmol of 2-hexanone in ethanol dropwise. Molar quantities of $3HT(CHO)_2$-KOH-hexanone were 1:2:1. System were kept 45 min under reflux at 65 °C. Crude were centrifugated to recover the polymer. Supernatant fluid containing a $3HT(CHO)_2$/polymer mixture were separated using CH_2Cl_2 and centrifugation. Polymer was introduced in acid solution and finally washed with water.

2.5 Synthesis of nanoparticles PbS/ZnS

PbS was obtained this way: 2 mL of $PbCl_2$ 30 mM and 2 mL of thioacetamide 30 mM were added to 50 mL of sodium citrate 3.0 mM and pH was adjusted to 7. The mixture was heated in a microwave oven on 20-20 seconds heating-rest cycles until 60 seconds; oven working at 80% of its total power. ZnS shell was got this way: 1 mL of 3-mercaptopropionic acid 0.18 M were added to the PbS np solution stirred for 1 min and then adjusting pH to 8. Mixture was translated to MW oven to be heated in 10-50 seconds heating-rest cycles and adding during rest 1 mL of both $Zn(OAc)_2$ and thioacetamide 1 mM, all this until 15 min of active heating.

2.6 Synthesis of composites

Mentioned polymerization was followed but a 5% w/w of PbS/ZnS nanoparticles were included before ketone addition, producing three hybrid polymer-nanoparticles composites.

2.7 Measurements

The structural analysis of products were performed with an H^1-MNR spectrophotometer (Varian MERCY 200) in which tetramethylsilane was used as the standard and an infrared spectrophotometer (Perkin Elmer SPECTRUM TWO), the reading was made in the solid form, therefore the ATR crystal was integrated, and the scan was carried out from 4000 cm^{-1} to 500 cm^{-1}.

The UV-Vis spectroscopy was performed in a

(Shimadzu UV-1800) spectrophotometer, scanning from1100 to 200 mm.

Gel permeation chromatography was performed in a chromatograph (YL Instruments YL9100 HPLC), using a YL9170 refractive index detector, and an Agilent Technologies PLGel column of 5 µm and dimensions of 7.5 x 300 mm. THF was used as the mobile phase, and a rate of 1 mL/min. The reference standard used was polystyrene.

The scanning electron microscope was performed in a microscope (JEOL JSM6701F) with secondary electron detector, in addition to a field emission scanning electron microscope (JEOL JSM-7600F) with both secondary electron and backscattered electron detectors (CINVESTAV Merida).

The thermal analyzes were performed on a DTA-TG unit (Linseis STA PT 1600), using a temperature ramp of 10° C/min until the 700° C.

The measurements of cyclic voltammetry and electrochemical impedance spectroscopy were processed in a Galvanostat potentiostat (AUTOLAB PGSTAT302N), using as support electrolyte TBaPF6 0.1 M, this is one of the most used electrolytes for organic techniques. The measurement was made at a scan rate of 0.01 V/s. Measurements were estimated with respect to the Fc^{+}/Fc redox couple (ferrocene)

The emission analysis of the polymers was carried out in a fluorescence spectrophotometer (Perkin Elmer LS55), in a solution of 0.5 mg of the polymer in 50 mL of THF and applying an excitation at 370 nm.

3. Results

Table 1. shows the ^{1}H-NMR values of different protons for Vilsmeier Haack product 3HTCHO. Here there is the evidence of presence of two structural isomers, 4-hexylthiophene-2-carboxaldehyde and 3-hexylthiophene-2-carboxaldehyde, such evidence arises since it can see *a* and *b* signals as doublets with integration for one proton, which ones are the expected for the two protons of 3-hexylthiophene-2-carboxaldehyde ring, meanwhile *c* and *d* singlets with integration for 0.33 proton are the expected in 4-hexylthiophene-2-carboxaldehyde. Singlets labeled as *e* and *f* appears shifted to 9.9 and 10.1 ppm, according to what would be expected for a carbonyl group and it reveals that a carbonyl have been added in both heterocycle rings. The presence of both isomers does not represent an obstacle for monomer synthesis, because isomers will undergo a second acylation reaction where free alpha carbon will participate, bringing a double substituted ring in two and five positions. Also, the characteristic peaks of methyl and methylene are presented in chemical shifts 2.5 and .8 respectively

Table 1. H-NMR values of different protons in the monomer

Proton	Integration	Chemical shift	Shape
a	1.15	7.1	Doublet
b	≈ 1.00	7.6	Doublet
c	0.33	7.4	Singlet
d	≈ 0.38	7.7	Singlet
e	0.32	9.9	Singlet
f	0.99	10.1	Singlet

Infrared interesting bands of 3HT, 3HTCHO and $3HT(CHO)_2$ are compared in Table 2, where it is evident the obtainment of a disubstituted heterocycle due to three signals. First, there are two carbonyl bands at 1654 and 1595 cm^{-1} due to different chemical environment that carbonyls experiences, whereas in 3HTCHO spectra it was observed only the band of 1654.
Furthermore, signal at 834 cm^{-1} corresponding to C–H bond out-of-plane torsion is decreased because the hydrogen loss of the ring when it gets a carbonyl group. Last, signal at 744 cm^{-1} corresponding to C–S bond stretching is decreased due to the stretching lower freedom for C–S bond when it is more substituted, in addition to this, signal is displaced to lower wave number by mesomeric effect that carbonyl groups generate.

Table 2. FT-IR spectrums comparison among 3HT, 3HTCHO and 3HT(CHO)2.

	3HT	3HTCHO	$3HT(CHO)_2$
C=O	--	1654 cm^{-1} (s)	1654 cm^{-1} (s)
	--	--	1595 cm^{-1} (s)
Ar–H	855 cm^{-1}(m)	857 cm^{-1} (w)	856 cm^{-1} (w)
	834 cm^{-1} (m)	840 cm^{-1} (w)	--
C–S	769 cm^{-1} (s)	744 cm^{-1} (m)	727 cm^{-1} (w)

The three polymers are dark brown solids at room temperature; they have a soft sweet sulphur odor. They all have poor solubility in methanol, acetonitrile, dichloromethane, and chloroform; however, they have partial solubility in acetone and tetrahydrofuran. They are insoluble in n-hexane. Notoriously, variation of secondary sidechain did not influence in the full solubility of the polymer. The main factor that rules the solubility is the polymerization grade; longer chains leads to insolubility.

Table 3 shows the polymers molecular weights. While PHT-B is an oligomer, PHT-P and PHT-H are polymers. Any given undesirable circumstance in the polymerization could have brought so wide polydispersity, and that's why more than a half of PHT-B molecules got like oligomer.

Table 3. Average molecular weights of the three polymers got by gel permeation chromatography.

	Mn (Da)	Mw (Da)	Mz (Da)	PDI
PHT-P	3,455	10,482	36,292	3.03
PHT-B	2,335	17,021	93,073	7.28
PHT-H	5,587	27,444	133,941	4.91

In general, it is observed that the average molecular weights of the three polymers grow as a larger ketone is used in the aldol condensation, which is an expected behavior in the size of the polymers that confirms that the side-chains are being integrated in the way proposed.

To prove the structural resemblance and the specific variations among them it was used Fourier transform infrared spectroscopy. Figure 2. shows the FT-IR spectrums for the three synthetized polymers; they all display the same signals for the thiophene ring and for the ketone-alkene conjugated section. Signals at 1591, 1643, 1668 and 1707 cm^{-1} are assigned to C=C and C=O bonds stretching. According to literature, ketone absorption bands appears primary between 1750 – 1650 cm^{-1} whereas alkene's bands are displayed between 1670 – 1600 cm^{-1} and these can appear at lower frequencies in conjugation with aromatics or carbonyls. Therefore, it is understood that bands at 1707 and 1668 cm^{-1} can be assigned to ketones with different chemical environment, whereas the signals at 1643 and 1591 cm^{-1} are characteristic of C=C bonds in conjugation with ketones in the backbone and with the thiophene rings, since alkenes in conjugation with aromatic rings displays bands at lower frequencies, and the presence of two bands confirms the conjugation with carbonyl groups.

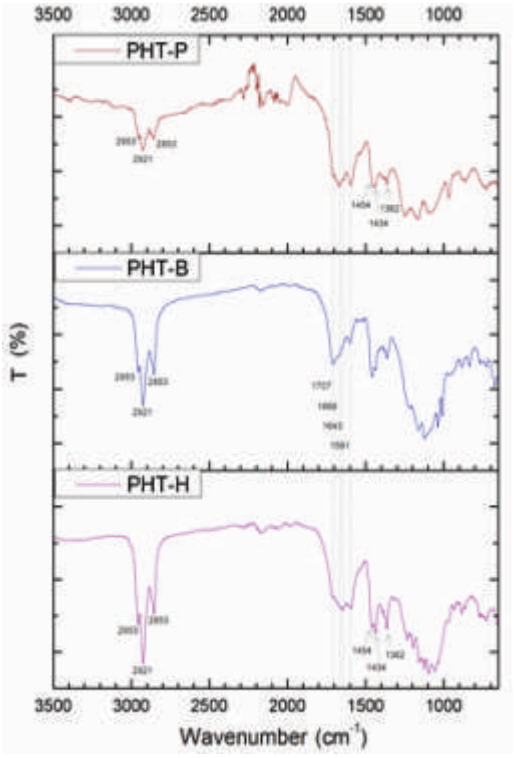

Figure 2. FT-IR spectrums for the PHT-P, PHT-B and PHT-H polymers

The absorbance spectra were of polymers were studied by UV-Vis spectroscopy. Figure 3 displays the spectrums of the polymers. Clearly, they show similar response to light, all of them have radiation absorption primary in visible region, with secondary absorption at ultraviolet region. They all show absorptions at 340, 279 and 248 nm, that correspond to charge transport among polymer chains, to perpendicular charge transfer among π orbitals of different chains, and to the π – π* electronic transitions, respectively.

With the obtained spectrums the optical band-gap energy (E_g^{op}) was estimated with the equation 1.

$$E_g^{opt} = \frac{c * h}{\lambda}$$ Equation (1)

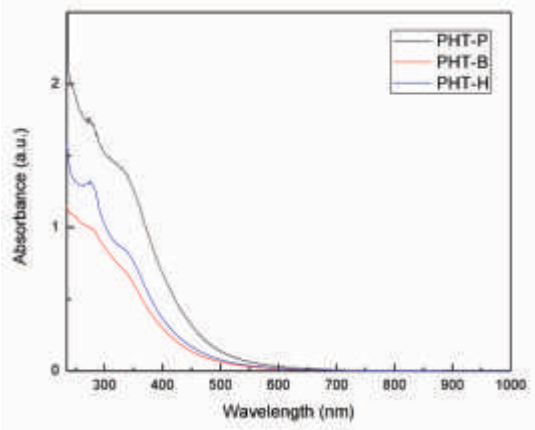

Figure 3. UV-Vis spectrums for the for the PHT-P, PHT-B and PHT-H polymers

Data was worked up to obtain an "squared absorbance vs energy" graph to get a better E_g^{op} value extrapolating from the first absorption to the *x* axis. Estimated E_g^{op} of the polymers are listed in the Table 4. Obtained values of E_g^{op} are greater than the proper of P3HT, but still belong to the range of semiconductors. The secondary sidechain that vary in the polymers did not influence in the E_g^{op}.

Table 4. Electronic properties of the polymer

Polymer	P3HT-P	P3HT-B	P3HT-H
Thickness (nm)	4,600	2,500	7,200
E_g^{opt} (eV)	2.64	2.71	2.70
Photoconductivity (S/cm)	$1.2x10^{-6}$	$2.3x10^{-6}$	$6.9 x10^{-7}$
HOMO (eV)	-6.25	-6.34	-6.58
LUMO (eV)	-3.39	-3.76	-3.65
E_g electrochemical	2.32	2.58	2.93
Electrochemical conductivity (S/cm)	$2.54x10^{-3}$	$3.1x10^{-3}$	$4.2x10^{-3}$

Figure 4 shows the emission spectrum obtained for two polymers obtaining an emission length of 533 nm for P3HT-P and 567 nm for P3HT-H, which correspond to a transition from π to π *. In addition, a second transition is observed around 670 nm which corresponds to an n-π * transition. Furthermore, it is observed that P3HT-P has a lower intensity, which indicates that it has a less marked recombination process.

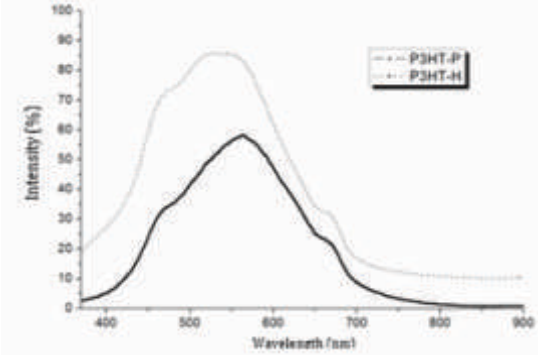

Figure 4. Emission spectra of P3HT-P and P3HT-H

Figure 5 shows images obtained from SEM of the polymers and the PbS/ZnS nanoparticles. For organic material, 5 a) P3HT-P and 5 b)P3HT-B stand out due to the fact that they present a greater homogeneity in the film, even so it presents protuberances due to its amorphous nature, instead in 5 c) P3HT-H shows more irregular areas.

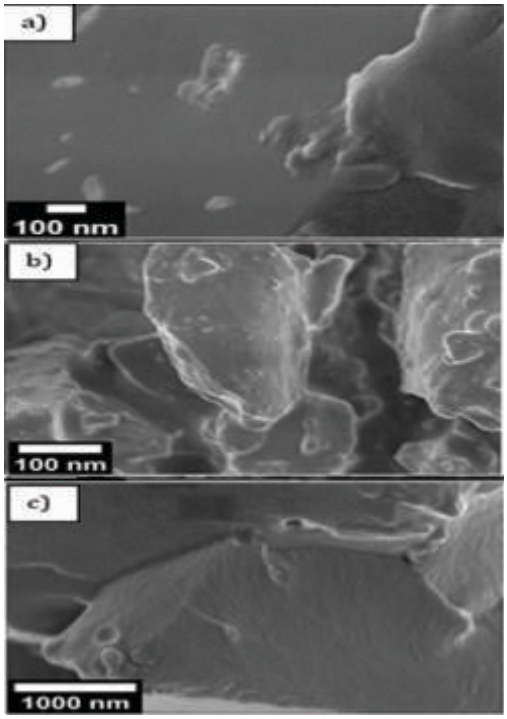

Figure 5. SEM images of a)P3HT-P with X50,000; b)P3HT-B with X20,000; c) P3HT-H with X30,00

Polymer films were elaborated by two ways: a)spin-coating, using chloroform to disperse the hybrid material on a Corning microscope glassslide as a substrate, and b) screen printing, using ethylenglycol, propylengllycol and terpynol to make a

paste,which were printing in the substrate. To calculate conductivity of polymers films by spin coating, a pair of 1.5 mm side-length silver contacts were painted on polymeric films; through them a voltage was applied, and an I-V curve was performed to obtain resistance from the slope of the I-V curve. The conductivity was calculated from the following equation:

$$\sigma = \frac{1}{R}\cdot\frac{L}{t.w} \qquad \text{Equation (2)}$$

where σ Is the conductivity, *R* is the resistance, *L* is the length of the contacts, *t* is the thickness of the deposited materials, and *w* is the contact width. The results are summarized in Table 4 in color blue. The conductivity results of the polymers are of the order of 10^{-6} S/cm; that values are comparable with the best ones of the first undoped polyconjugated systems, which span $10^{-6} – 10^{-9}$ S/cm,[23]. However, a previous synthesis of PHT-P' had given a conductivity of 10^{-3} S/cm, and that PHT-P' had a M_n of 4,847 Da and a M_w of 12,024 Da. It was notorious that PHT-P' was completely soluble in THF. Therefore, it is concluded that the synthesis conditions are a key factor on the polymer properties like solubility and conductivity at least.

In the screen printing´s films the conductivity were calculate by electrochemical impedance spectroscopy. In the figure 9 we have the impedance spectra which is an electrochemical technique based on the disturbance of the equilibrium of a system through the application of an amplitude of potential AC (alternating current). In order to make the interpretation of the data obtained using the Nyquist and Bode graphs easier, the use of equivalent electrical circuits has been established as a strategy, which should describe as accurately as possible the behavior described by these graphs. Furthermore, each component of the circuit must be related to one of the System parameters. For the P3HT-P film, figure 9 a) a Nyquist graph is obtained that describes a semicircle and a straight line, this behavior can be associated with the Randles circuit and an element Warbug is added, which describes the mass transfer (straight line).

$$\sigma = \frac{1}{R_s}\frac{L}{A} \qquad \text{Equation (3)}$$

Where L is the distance between electrodes (cm), Rs is the resistance between solution and conductive polymer (ohm) and A is thw Working electrode area (cm^2). Substituting the values in equation 3, a conductance value of $2.54x10^{-3}$ S/cm is obtained. For the P3HT-H film it does not describe a behavior as such of a semicircle, but it also starts from the Randles circuit modified with constant phase element (CPE), substituting the values to equation 1 to obtain a conductance value of $4.2x10^{-3}$ S/ cm

The cycle voltammetry was used to estimate the HOMO LUMO positions of the P3HT derivatives (Figure 6). During the measurement, the oxidation and reduction processes were measured separately because the reduction process caused changes in the electrochemical properties of the film, since it was observed that the Film was dissolved by the applied potential. The value of the HOMO position was estimated with equation 1, that of the LUMO position with equation 4 and the band gap with equation 5 with respect to the redox torque Fc + / Fc (ferrocene) and is taken as the energy value vs . vacuum value -5.1 eV together with this value and the equations can estimate each position and equation 6 was used to obtain the prohibited bandwidth.

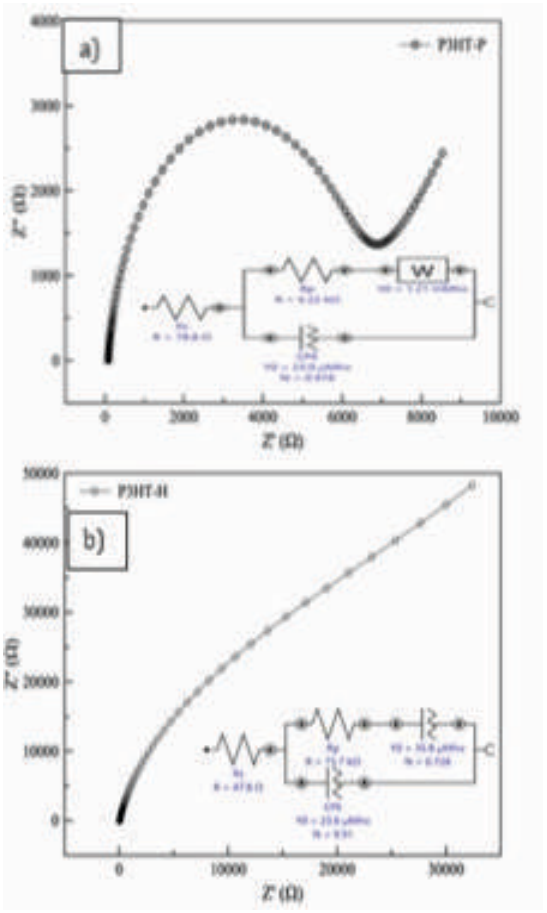

Figure 6. Nyquist graphs and equivalent electrical circuit of the polymers a) P3HT-P y b) P3HT-H

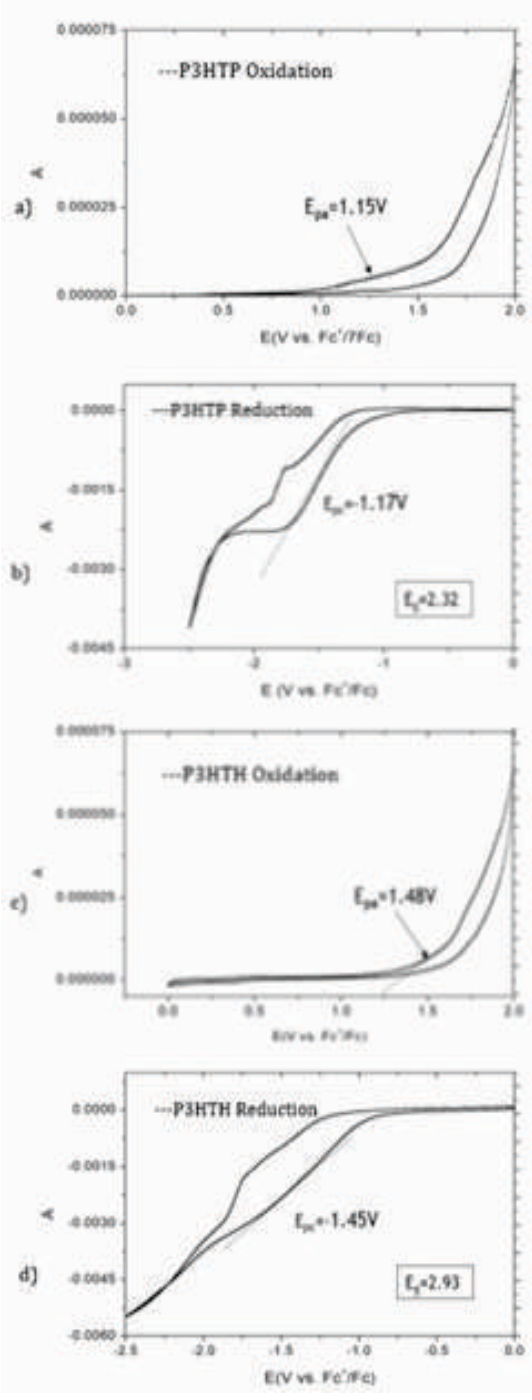

Figure 7. Cyclic Voltammograms of Polymers: a) P3HT-P oxidation process b) P3HT-P reduction process, c) P3HT-H oxidation process d) P3HT-H reduction process

$$E_{HOMO} = -e[E_{ox}^{onset} + 5.1] \quad \text{Equation (4)}$$

$$E_{LUMO} = -e[E_{red}^{onset} + 5.1] \quad \text{Equation (5)}$$

$$E_g = |E_{HOMO} - E_{LUMO}| \quad \text{Equation (6)}$$

The measurements of the oxidation and reduction processes were made separately as shown in Figure 8, in order to determine the E_p^a and E_p^c of the anode and cathodic branch, this due to the oxidative nature of the polymer because when applying a reduction potential the film dissolves affecting the cycle reading.z

In both voltammograms as seen in images 7a, 7b, 7c and 7d, the most defined process is the oxidation, as mentioned, it has a greater influence on the electrochemical characteristics of the conductive polymer film. The potential of the anode branch is located around 1.15 V (HOMO -6.25 eV) while in the cathodic branch (reduction) a value of -1.17 V (LUMO -3.93 eV) is estimated vs. the Fc + / Fc redox pair. Obtaining an Eg of 2.32 eV, said value is within the range of Eg estimated for conductive polymers. While the P3HT-H presents higher values HOMO -6.58 eV and LUMO of -3.65 eV with an estimated value of Eg of 2.93 eV.

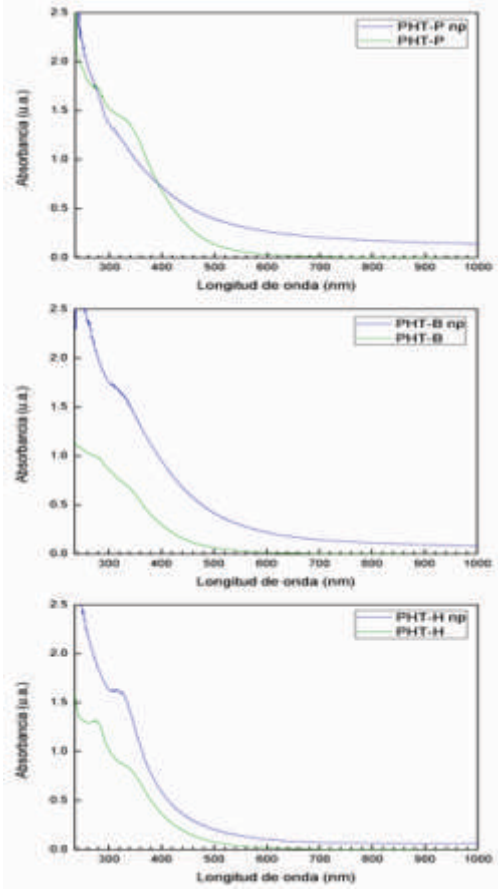

Figure 8. UV-Visible absorption spectrums of composites

Polymers derived from 3-hexylthiophene generally absorb radiation at wavelengths lower than 600 nm; it is common that they do not take advantage of radiation from yellow to infrared. The behavior of the polymers PHT-P, PHT-B and PHT-H in their radiation absorption capacity followed this trend, so the addition of PbS/ZnS nanoparticles was aimed at, in addition to achieve a hybrid p-n material, improve the absorption of radiation to greater wavelengths. Figure 8 shows UV-Visible absorption spectrums of composites and their comparison with initial polymers. Analyzing the absorption behavior for the three cases, it is obvious that the addition of nanoparticles improved the uptake of radiant energy in the range of 500 to 1000 nm, where absorption was zero. It is also observed that the absorption in the ultraviolet region is improved by the addition of nanoparticles. It is noteworthy that the addition of nanoparticles in these experiments was only 5% by weight, which leads one to infer that the absorption can still be improved by adding a greater quantity of PbS/ZnS nanoparticles or even some other nanoparticulate semiconductor with properties similar to the mentioned one.

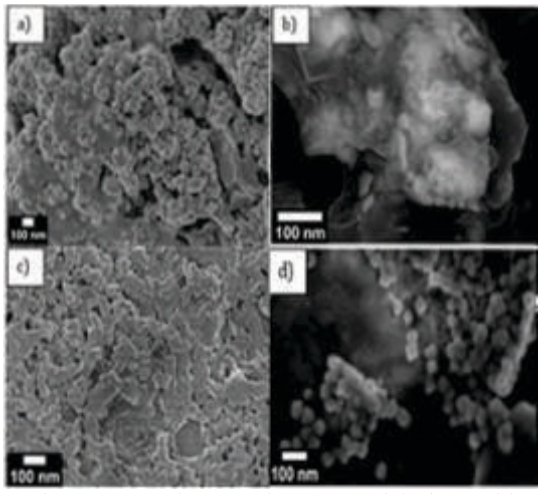

Figure 9. SEM images of a) P3HT-P/PbS/ZnS with X50,000; b) P3HT-B/ PbS/ZnS with X20,000 and c) P3HT-H/ PbS/ZnS with X10,00 and d) PbS/ZnS NPs

In the Figure 9 Inorganic nanoparticles are shown in a core /shell configuration, with a average size of 20 nm. For P3HT-P/Pbs/ZnS (Fig. 8a)makes evident polymer areas with a notorious presence of nanoparticles cumulus randomly incrusted in some regions of the polymer, the NPs cumulus has an average size of 46.7 nm(20 nm greater than pure NPs).The Fig. 8b shows thr P3HT-B/PbS/ZnS image obtained with a detector of backscattered electrons which allows to see in a same surface different scale of brightness/darkness in the presence of different atomic masses of the elements that form it. With this it can be noted that there is a presence of nanoparticle cumulus embedded in the polymeric matrix due to the different gray scale visible on the surface, this difference of shades being the presence of lead, sulfur and zinc. In Fig.8c image of P3HT-H/PBs/ZnS shows the granules of the polymer with nanoparticles the point cumulus.

Composite films were made by depositing the material via spin-coating to evaluate electrical conductivity in a manner like that done with pure polymers. Table 6 shows that the addition of the PbS / ZnS nanoparticles to the polymers substantially improves the electrical conductivity, specifically by 7 orders of magnitude, with respect to the polymers without nanoparticles. For the PHT-H: PbS / ZnS there is a smaller increase, in this case it is contemplated that the estimate could be altered by the same measurement technique since when putting the cables on the contacts it was felt that the silver contact that had been painted, it was possible to move a little, which evidenced the little firmness with which the film of this polymer was deposited on that substrate.

Table 5. Conductivity of polymer and composites.

Polymer	Conductivity of polymer pure ($S \cdot cm^{-1}$)	Conductivity of Composite ($S \cdot cm^{-1}$)
PHT-P	1.8×10^{-6}	7.3×10^{1}
PHT-B	2.7×10^{-6}	2.2×10^{1}
PHT-H	2.8×10^{-6}	5.8×10^{-3}

Conclusions

Three new semiconducting polymers were created and three composites adding PbS/ZnS nanoparticles to the formers. The three synthesized semiconducting polymers showed poor solubility in most organic solvents, with acetone and tetrahydrofuran being those with the highest partial solubility; in general, the variation in one of its side chains has little influence on its solubility, this is because the chain is too short to contribute to the solubility compared to what hexyl contributes in P3HT. Although the E_g value of the three polymers was greater than that of P3HT, the estimated conductivity for all three is adequate for a semiconductor. The values of HOMO, LUMO and $Eg^{electrochemical}$ for both polymers were obtained from CV measurements showing a good values for it application in solar cells. Also the conductivity values were obtained by EIS showing the P3HT-P with the highest value. Comparing Tables 3 or 4, the values obtained by electrochemical techniques demonstrate that the polymer has a higher conductivity value and a lower E_g than the E_g^{op}.

References

1. Cabriales, G. & González, G. Nuevo material luminiscente para dispositivos optoelectrónicos.

Ingenierías. 2004, Vll(24), 6–11. http://ingenierias2.uanl.mx/77/index.html
2. Dai, L. Intelligent Macromolecules for Smart Devices: From Materials Synthesis to Device Applications; Springer; 2004; pp 41-43. https://doi.org/10.1007/1-85233-849-0_2
3. Spanggaard, H. and Krebs, F.C. (2004) A Brief History of the Development of Organic and Polymeric Photovoltaics. Solar Energy Materials and Solar Cells, 83, 125-146.
4. http://dx.doi.org/10.1016/j.solmat.2004.02.021
5. Reiss, P., *et al*. Nanoscale. 2011, 3, 446–489. https://doi.org/10.1039/C0NR00403K
6. Cordovilla, C., *et al*. ACS Catal. 2015, *5* (5), 3040–3053. https://doi.org/10.1021/acscatal.5b00448
7. Pourjafari, D.; Vazquez, A.; Cavazos, J.; Gomez, I. Soft Materials. 2014, 12, 380–386. https://doi.org/10.1080/1539445X.2014.934842
8. Baskar, R., *et al*. RSC Advances. 2013, 3, 17039-17047. https://doi.org/10.1039/C3RA42424C
9. Manouras, T. & Vamvakaki, M. Polymer Chemistry. 2017, 8, 74-96. https://doi.org/10.1039/C6PY01455K
10. Huang, X., *et al*. J. Mater. Chem. 2012, 22, 22488-22495. https://doi.org/10.1039/C2JM34340A
11. Bao, Z., *et al*. Appl. Phys. Lett. 1996, 69(26), 4108–4110. https://doi.org/10.1063/1.117834
12. Boucle, J., *et al*. J. Mater. Chem. 2007, 17, 3141–3153. DOI: 10.1039/b706547g
13. Xu, T. & Qiao, Q. Energy & Environmental Science. 2011, 4, 2700–2720. https://doi.org/10.1039/C0EE00632G
14. Mohd-Nasir, S. N. F., *et al*. International Journal of Photoenergy. 2014, 370160. https://doi.org/10.1155/2014/370160
15. Vapaavuori J et al. **J. Mater. Chem. C**, 2018,**6**, 2168-2188. https://doi.org/10.1039/C7TC05005D
16. Han, S., *et al*. The Solid Films. 2015, 576, 38-41. https://doi.org/10.1016/j.tsf.2014.12.025
17. Pan X et al. Chem. Soc. Rev., 2018,47, 5457-5490. https://doi.org/10.1039/C8CS00259B
18. Seoyoung Kim, Doyoung Lee, Jungho Lee, Yongjoon Cho, So-Huei Kang, Wonbin Choi, Joon Hak Oh, Changduk Yang. Diazapentalene-Containing Ultralow-Band-Gap Copolymers for High-Performance Near-Infrared Organic Phototransistors. Chemistry of Materials 2021, 33 (18) , 7499-7508. https://doi.org/10.1021/acs.chemmater.1c02409
19. Mooney M et al. ***J. Mater. Chem. C***, 2020,**8**, 14645-14664. https://doi.org/10.1039/D0TC04085A
20. González, V., Arias, E. y Esquivel, E. Relación estructura–luminiscencia en aductos de condensación aldólica, Ingenierías. 2007, X(34), 69–75.
21. Ando, W., *et al*. Science of Synthesis: Houben-Weyl Methods of Molecular Transformations, Vol. 9: Fully Unsaturated Small-Ring Heterocycles and Monocyclic Five-Membered Hetarenes with One Heteroatom. Editor Georg Thieme Verlag, 2014; pp 351.
22. Murad, A.R., Iraqi, A., Aziz, S.B., Abdullah, S.N., Brza, M.A. Polymers 2020, 12(11), 2627; https://doi.org/10.3390/polym12112627.
23. Nalwa, H.S. Handbook of Advanced Electronic and Photonic Materials and Devices: Liquid crystals, display and laser materials. Vol. 7. Academic Press, 2001; pp 47-48.
24. Cheng, Y.J., Yang, S.H., y Hsu, C.S. (2009). Synthesis of conjugated polymers for organic solar cell applications. Chemical Reviews, 109(11), 5868– 5923. https://doi.org/10.1021/cr900182s.